Development of a Finite Element Based Hall Thruster Model for Sputter Yield Prediction*†

Subrata Roy and Birendra Pandey
Computational Plasma Dynamics Research Laboratory
Kettering University
1700 West Third Avenue
Flint, MI 48504
810-762-9949
sroy@kettering.edu

IEPC-01-49

Modeling the Hall thruster for sputter yield prediction is of considerable interest to the electric propulsion community. This paper documents the status of a finite element based computational development for modeling unsteady plasma flow in the acceleration channel of a stationary plasma thruster (SPT). The results are validated with the available test data and compared with the reported results of particle-in-cell (PIC) method in the literature. Computational challenges are discussed. The lifetime issues also are considered.

Introduction

Hall thruster (also known as stationary plasma thruster (SPT) or closed drift thruster) experimentation started in the early 60's and due to the diligent Russian effort became an enabling technology for on-board propulsion in many LEO and GEO satellites [1]. Present day Hall thrusters offer specific impulses ranging 1600s to 2000s with 80mN to 200mN thrust for power ranging 1.5kW to 4.0kW. Utilizing xenon propellant, NASA GRC aims for increasing the efficiency of the Hall thruster while having a lifetime of close to 8000hrs. This is a challenge, as the choice of thruster size requires an optimum selection between efficiency and lifetime [2]. The physics inside the Hall thruster have to be reasonably well understood in order to make any significant change in efficiency without compromising the lifetime. Despite ample theoretical and experimental efforts published in the literature, a recent study [3] recognizes the need for an acceptable computational model that captures the details of electrons and plasma dynamics inside the thruster annular cavity.

The electric propulsion devices are more challenging in comparison with chemical propulsion devices; as not only obtaining the test results under real flight conditions are difficult, but also the interaction of the plasma plumes with the spacecraft makes the problem highly non-linear. However, the electric propulsion devices allow for lower propellant mass by generating higher exhaust velocities than is otherwise possible with chemical rockets. Hall thruster has emerged as an attractive electrostatic propulsion device and is under development in several countries across the globe due to its potential for future primary propulsion applications. The reason for its popularity lies in its good performance. For example, it has superior thrust (~80 mN) than other type of stationary thrusters since the acceleration is not inhibited by the space charge field in quasi-neutral plasma [4-5]. The efficiency of a typical optimized Hall thruster is about 50% or more and can operate over a wide range of currents.

The Hall thruster has an annular geometry with a dominant radial magnetic field. The presence of a strong radial field inhibits the transverse motion of the electrons as they are virtually glued to the radial field lines, since their gyration radius is negligible in comparison with the width of the channel. Furthermore, the electrons behave like an ideal gas as their collision mean free path is large, implying that

* Presented as Paper IEPC-01-49 at the 27th International Electric Propulsion Conference, Pasadena, CA, 15-19 October, 2001.

there is no motion in the axial direction. The resulting high impedance of the electrons in the axial direction helps to maintain an electric field between anode and cathode. The ions, on the other hand have a large gyration radius and therefore, will behave as if there is no radial magnetic field. This will result in ions streaming out of the device, accelerating down the potential like unmagnetized plasma.

Numerical simulation is an invaluable tool as it can mimic the real flight condition. The numerical studies of the plasma dynamics of a Hall thruster is essential and has been carried out recently by several authors in the framework of hybrid as well as fluid models [6-10]. These studies are aimed at providing better understanding not only of the performance, but also of design issues. Despite great advances in our understanding of the plasma dynamics of a Hall thruster, there is a need to further investigate the subject as this will facilitate the improvement and optimization of the thruster design. In the present work, employing numerical simulation, we study the physics of the acceleration process in the Hall thruster. We anticipate that the numerical model will provide a clear understanding of the underlying physical phenomena of Hall thruster plasma. We represent the plasma in a two dimensional hydrodynamic model in the presence of a radial and axial magnetic field, and an axial electrostatic field. The result predicted by the model is supported by the experimental data.

This paper documents the status of the development of a computational framework for efficient plasma flow simulation for a working gas (xenon) inside the Hall thruster. It compares existing physics-based particle-in-cell (PIC) type models [11,12] with modern mathematical analyses of the discrete methods used to solve the underlying partial differential equations. The numerical simulation is based on the two-momentum, single-temperature (TMST) fluid flow based equation that is an extension of [13]. These time accurate finite element method results are comparable to the hybrid PIC [4]. Note that [14] found no noticeable effect of Monte Carlo simulation and upwind integration scheme except for excess diffusion in the ion distribution in velocity space. Unlike traditional upwind methods, however, non-linear TMST does not introduce any unnecessary diffusion to distort the solution. The computational study is compared with reported data in [11,12,15] and benchmarked with the testing effort at GRC facility. Presented results will specifically focus on the near-wall conductivity and understanding the effect of different physical parameters on the efficiency of the thruster.

Theoretical Issues

It is well known that in a Hall thruster, the plasma is a partially ionized mixture of electrons and mostly, singly ionized and unionized inert gas. The dynamics of such plasma is quite complicated. Therefore, we make some simplifying assumptions before the dynamics of all the three components can be considered. We consider a two-fluid, hydrodynamic equation to model the plasma. Although, the geometry of the Hall thruster is three-dimensional, we shall ignore any variation in the axi-symmetric direction. The following set of compressible, two-fluid equations may describe the dynamics of thruster plasma,

$$\frac{\partial \rho_\alpha}{\partial t} + \nabla \cdot (\rho_\alpha \mathbf{V}_\alpha) = 0 \qquad (1)$$

$$\frac{\partial \rho_i \mathbf{V}_i}{\partial t} + \nabla \cdot (\rho_i \mathbf{V}_i \mathbf{V}_i) = Zen_i \mathbf{E} - \nu_c (\rho_i \mathbf{V}_i) + \frac{m_e}{m_i} \nu_{ie} \rho_i (\mathbf{V}_e - \mathbf{V}_i) \qquad (2)$$

$$\frac{\partial \rho_e \mathbf{V}_e}{\partial t} + \nabla \cdot (\rho_e \mathbf{V}_e \mathbf{V}_e) = -\nabla p - \nu_{ei} \rho_e (\mathbf{V}_e - \mathbf{V}_i) + \frac{e\rho_e}{m_e} (\nabla \phi - \mathbf{V}_e \times \mathbf{B}) \qquad (3)$$

$$\frac{\partial e}{\partial t} + \nabla \cdot (e\mathbf{V}_e) = -p \nabla \cdot \mathbf{V}_e + \nu_{ei} \rho_e (\mathbf{V}_e - \mathbf{V}_i)^2 \qquad (4)$$

The above set of equations is not closed and therefore, needs to be complemented with a thermodynamic relation between internal energy e and pressure p, i.e., $p = (\gamma - 1)\, e$, where γ is the ratio of the specific heats and is taken as 5/3. Here $\mathbf{V}_e$, $\mathbf{V}_i$ are the electron and ion velocities, respectively. **E** and **B** are the imposed electric and magnetic field in a quasi-neutral plasma, and density ρ_α is the product of mass density m_α and number density n_α of the αth particle with $\alpha = e$ and i, $\nu_{e,i}$ is the electron-ion collision frequency, ν_c is the ion charge exchange collision frequency, e is the electron charge and Z is the ionicity and p is the thermal pressure of the electrons.

In the continuity equation (1), we assume that there is no source or sink term, for both electrons and ions. This assumption may not be justified very close to the

wall of the thruster where the sputtering and recombination may become important. However, the dynamics of the plasma will be little affected far off from the wall due to the sputtering and recombination. Thus, the zero source and sink term in continuity equation may be a valid starting assumption to study such a plasma. Also, if we visualize the constant puffing of noble gas to the chamber, we can imagine a scenario where, for the dynamically interesting time scale, namely over the pulse time, the plasma can be assumed to have negligible loss and any loss is balanced instantaneously.

The thruster plasma is assumed to be quasi-neutral as Debye length, which is the measure of spatial scale over which plasma may have a self electric field, is ~0.02 mm near the anode and 0.1 mm in parts of the plume [6], considerably smaller scale than the scale we model in the present investigation. Therefore, assumption of quasi-neutrality is reasonable except in the Debye sheath near the wall. In the quasi-neutral plasma, Poisson's equation is not solved and potential will be extracted from the electron momentum equation along the magnetic field. Furthermore, we shall consider only singly charged ions. This is a plausible assumption as we can see from the following reasoning.. As soon as neutrals loose an electron, they will experience a very strong electric field that will sweep them away from the discharge zone before another ionization can take place. Therefore, most of the thruster plasma will have singly charged ions with a very low density of multiple-charged ions that may be caused by the impact with the very energetic electrons. We note that apart from energetic electrons, whose density is generally low, the cross section for multiple ionization in a single collision is small in comparison with the single ionization cross section.

In the ion momentum equation, the ion momentum exchange due to collision with electrons (last term in equation (2)) will not be significant as ion mean free path is generally larger (~30 cm) than the size of the thruster (~3 cm). Also, we are considering ions as unmagnetized, since the gyration radius of ions are typically 100 cm for a 200G field with an ion velocity 1.6×10^6 cm/s [2]. Therefore, it is reasonable to assume ions to be unmagnetized and ignore the effect of magnetic field on the ion transport. Further, we shall assume ions to be cold. The ion charge exchange term acts as a drag force in the momentum equation.

The dynamics of the electron is determined by the pressure gradient, by the electric and magnetic forces and by collisional exchange of momentum in equation (3). However, the contribution of the collisional term to the momentum exchange will be negligibly smaller in comparison with the remaining terms and will be dropped. In the electron energy equation (4), the energy source term in general is

$$S = m_e n_e \nu_{en}(\mathbf{V}_n - \mathbf{V}_e)^2 + m_e n_e \nu_{ei}(\mathbf{V}_i - \mathbf{V}_e)^2 + 3m_e n_e \nu_{en}(\mathbf{V}_{nt}^2 - \frac{m_e}{m_n}\mathbf{V}_{et}^2) + 3m_e n_e \nu_{ei}(\mathbf{V}_{it}^2 - \frac{m_e}{m_i}\mathbf{V}_{et}^2) \quad (5)$$

where $\mathbf{V}_{\alpha t} = \sqrt{k_B T_\alpha / m_\alpha}$ is the thermal velocity of the αth species. We have ignored the terms due to electron-neutral momentum exchange and due to the exchange of energy due to random thermal component and have retained the most dominant contribution, due to the exchange of the mean flow energy between electrons and ions in our investigation. Based on the simulation [15], the average ion energy remains nearly constant in the channel. Therefore the ion energy is assumed constant in our model.

In the presence of an applied axial electric field E_z and the radial magnetic field B_r, the electrons experience a drift in the θ-direction and therefore constitute a Hall current.In the axial electron current, which results from collisions, sputtering and potential fluctuation may be completely inhibited by the presence of a strong magnetic field. As a result, the current $j_z \approx j_i$, i.e., electric field supplies mainly energy to the ions. Assuming an **E**×**B** velocity for electrons, the Hall current per unit radius is

$$J_H \approx en_e \int_0^r E/B dr \approx en_e \phi_d / B \quad (6)$$

where, ϕ_d is the discharge potential. Note that discharge potential is the sum of the column potential drop ϕ, the cathode fall potential and the possible potential drop in the plasma region next to the exhaust and outside the cylinders. For $j_i \approx en_e v_i$, for quasineutral ($n_i \approx n_e$) plasma, we have

$$J_H \approx j_i V_\theta / B v_i \approx j_i \sqrt{\frac{m_i \phi_d}{2eB^2}} \quad (7)$$

where use has been made that maximum ion velocity is $v_i=(2eV_d/m_i)^{1/2}$. Clearly, for a given magnetic field,

$J_H/j_i \sim \sqrt{V_\theta}$. For an efficient operating system, current is carried by the ions and ions attain maximum velocity.

The radial magnetic field distribution has been assumed to be bell shaped in the axial direction, reaching a maximum near the pole pieces and decreasing both near the anode and the exit end of the thruster. The following profile for the radial magnetic field has been assumed $B_r(r) = B_0 \exp(-r^2)$. The ensuing potential distribution (and the resultant accelerating electric field) will be in the region of maximum magnetic field strength. As discussed above, the plasma is assumed quasi-neutral and thus, the potential cannot be obtained by solving Poisson's equation. The electron equation of motion (3) is integrated along the magnetic field to deduce the expression for potential,

$$\phi(z,t) = \phi_0 - \frac{k_B T_e}{e} \ln \frac{n_e(z,t)}{n_{e0}} \qquad (8)$$

where n_{e0} is the background plasma density when potential approaches some base value ϕ_0. It should be noted that this potential $\phi(r,t)$, which is imposed in the model is the potential along the column and is not the discharge potential. This is the "thermalized" potential" within the discharged plasma. Assuming that the parallel conduction of the electron along the magnetic field line is zero, so that the potential build up is not short circuited, it follows that the thermalized potential is constant along the magnetic field lines.

Finite Element Based Modeling

A general formulation for (1)-(4) may be expressed as $L(\mathbf{U})=0$, where $\mathbf{U}=\{\rho_\alpha, \mathbf{V}_i, \mathbf{V}_e, e\}^{\mathrm{T}}$ and L is a differential operator. The weak statement underlines the development of the range of CFD algorithms. Such an integral statement associated with (1)-(4) is

$$\int_\Omega w L(\mathbf{U}) d\Omega = 0 \qquad (9)$$

where w denotes any admissible test function [16]. Thereafter, the finite element (FE) spatial semi-discretization of the domain Ω of (1)-(4) employs the mesh $\Omega^h = \cup_e \Omega_e$ and Ω_e is the generic computational domain. Using superscript "h" to denote "spatial discretization," the FE weak statement implementation for (9) defines the approximation as

$$u(x_j) \approx u^h(x_j) = \sum_e u_e(x_j) \text{ and } u_e(x_j) = N_k \mathbf{U}_e$$

where subscript e denotes elements, and the trial space FE basis set $N_k(x_j)$ typically contains Chebyshev, Lagrange or Hermite interpolation polynomials complete to degree k, plus perhaps "bubble functions" [16].

The spatially semi-discrete FE implementation of the *weak statement* WS^h for (9) leads to

$$WS^h = S_e \left(\int_{\Omega_e} N_k L_e(\mathbf{U}) d\tau \right) \qquad (10)$$

S_e symbolizes the "assembly operator" carrying local (element) matrix coefficients into the global arrays. Application of Green-Gauss divergence theorem in (10) will yield natural homogenous Neumann boundary conditions and the surface integral that contains the unknown boundary fluxes wherever Dirichlet (fixed) boundary conditions are enforced.

Independent of the physical dimension of Ω, and for general forms of the flux vectors, the semi-discretized weak statement of (9) always yields an ordinary differential equation (ODE) system:

$$\mathbf{M}\, d\mathbf{U}/dt + \mathbf{R}(\mathbf{U}) = \mathbf{0}, \qquad (11)$$

where $\mathbf{U}(t)$ is the time-dependent finite element nodal vector. The time derivative $d\mathbf{U}/dt$, is generally replaced by using a θ-implicit or n-step Range-Kutta time integration procedure. In (11), $\mathbf{M} = S_e(\mathbf{M}_e)$ is the "mass" matrix associated with element level interpolation, $\mathbf{R}$ carries the element convection information and the diffusion matrix resulting from genuine (not for Euler) or numerical elemental viscosity effects, and all known data. For steady state, (11) is usually solved using a Newton-Raphson scheme:

$$\mathbf{U}_{n+1}^{i+1} = \mathbf{U}_{n+1}^{i} + \Delta\mathbf{U}^{i} = \mathbf{U}_n + \sum_{p=0}^{i} \mathbf{U}^{p+1}, \text{ where}$$

$$\Delta\mathbf{U}^{i} = -\left[\mathbf{M} + \theta \Delta t (\partial\mathbf{R}/\partial\mathbf{U})\right]^{-1} \mathbf{R}(\mathbf{U})$$

The obvious numerical issues will be associated with calculation of the "jacobian" $\partial\mathbf{R}/\partial\mathbf{U}$ and inversion of the $\mathbf{M}+\theta\Delta t(\partial\mathbf{R}/\partial\mathbf{U})$ matrix with sufficient accuracy. We have employed an explicit (θ=0) time stepping procedure for this paper.

Results and Discussion

Test Conditions:

In Fig. 1., a schematic diagram of the NASA 120-M Hall thruster is given. The main components of this

magnetic layer thruster consist of an inner coil with magnetic pole, outer coils with the outer pole pieces, a boron nitride discharge channel, the non-magnetic gas distributor and anode, and the outer and inner magnet screens. The plasma column is contained within two coaxial dielectric cylinders that constitute the discharge channel, with the anode at one end of the channel and the exit at the other end of the channel.

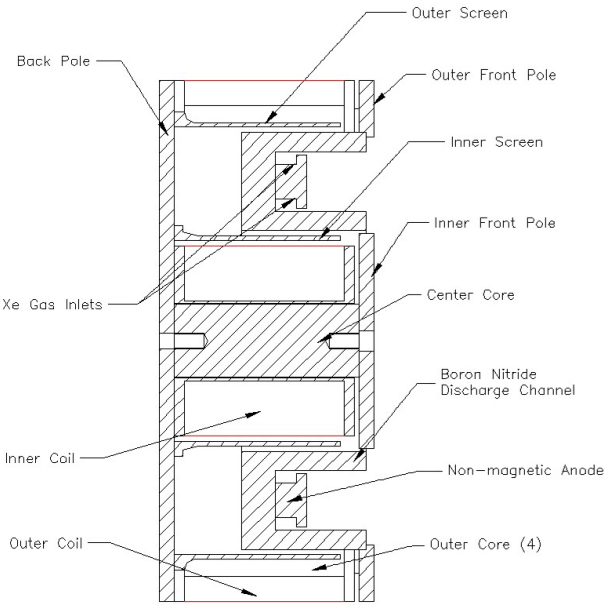

Figure 1. Schematic of NASA 120M Thruster.

In the present investigation, we shall focus on the plasma behavior inside the channel. The propellant used in NASA 120-M is Xenon, which is injected at a nominal rate of 5.87 mg/s from the anode. The cathode flow rate is 0.87 mg/s. As the length and width of the channel are relatively small (~2 cm), and the gas density at the point of injection is $\sim 10^{13}$ cm^{-3}, a magnetic field is necessary to confine the electrons. The effect of the magnetic system, consisting of a series of electromagnetic coils employed inside the inner cylinder and outside the outer cylinder, is a radial magnetic field with a maximum next to channel exit. The presence of this radial magnetic field inhibits electrons flow to the anode and in the process, enhances ionization due to electron impact considerably. The voltage drop between the anode and the external cathode is nominally 300 Volts. The radial magnetic field decreases from a maximum of about 200G near the channel exit to a much lower value near the anode. At these operating conditions the thruster operates at approximately 2 kilowatts with performance comparable to other state-of-the-art Hall thrusters. The static radial and axial magnetic field distribution measured within the discharge channel is shown in Figure 2 [17]. Corresponding thrust is measured as 102.6 mN.

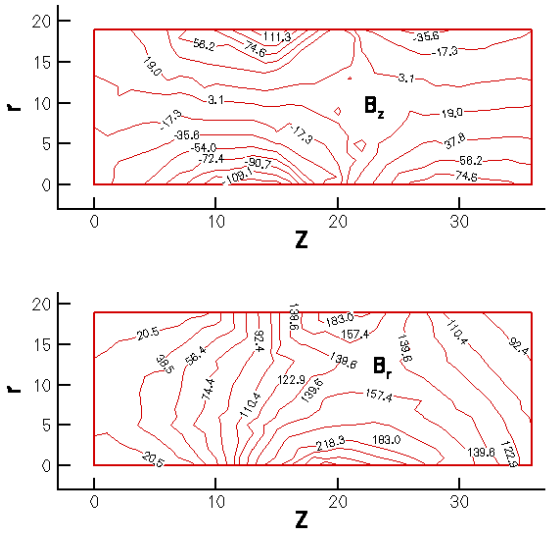

Figure 2. Measured magnetic field (B_z and B_r) inside the thruster acceleration channel and plume.

Numerical Results:

We model an axisymmetric cylindrical thruster plasma by a slab *r-z* geometry where, *r* corresponds to the radial direction whereas *z* corresponds to axial direction. The θ–direction is along the azimuth. We shall consider a two-dimensional magnetic field geometry, with the radial and axial components. Furthermore, it assumed that the radial field is dominant in comparison with the axial field. This assumption is supported by the experimental investigation of the magnetic field distribution near the Hall thruster [18,19]. The set of equation (1)-(4) has been solved using a 2.5 dimensional hydrodynamic code. The computational box spans (r: 0,1)×(z: -1, 1) and contains 36 cells in the axial and 19 cell in the radial directions. The channel wall no-slip boundary extends for 19 axial cells along the top and bottom of the mesh (Fig.3).

The ion and electron density boundary conditions consist of fixing them at the anode plane (inlet) and leave them floating at the exit plane, i.e., $\rho_\alpha = \rho_{\alpha 0}$ at the anode. We consider rigid wall condition for the *r*- and *z*-components of the ion and electron velocities on the channel wall, i.e., $V_{\alpha r} = 0 = V_{\alpha z}$. The drift velocity of the electron V_θ is calculated at the inlet from the profile of the magnetic field B_r and the potential. The *z*-component of electron and ion velocities are

assumed to be non-zero at the anode plane, i.e., $V_{\alpha z} = V_{\alpha z0}$ at the inlet and rigid wall condition at the top and bottom boundary. The electron energy boundary condition consists of fixing the electron mean energy at the exit plane, i.e., $e(z=1) = e_0$ and imposing a homogeneous Neumann (zero slope) condition at the inlet.

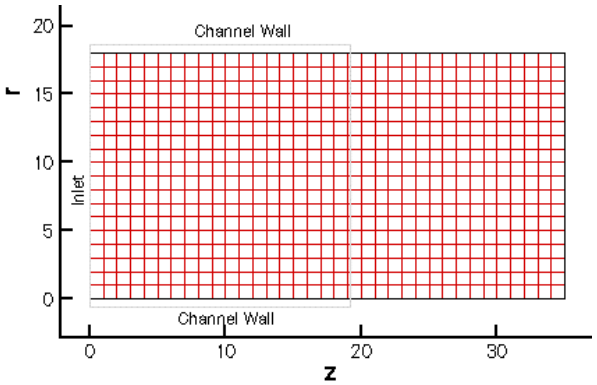

Figure 3. Computational mesh

We assume that the ions are cold [15]. However, we reemphasize that the ion temperature and consequently, ion pressure gradient plays an important role in accelerating the ions inside the channel. Therefore, the result being presented here is for a thermal electron and cold ions. Despite the inclusion of charge exchange collision, the momentum exchange between electrons and ions is ignored as these terms are much smaller than the remaining terms of the respective momentum equation.

We also assume that at the inlet, the ions have nonzero mass density. As the Xenon is puffed in the channel, it undergoes immediate ionization. Therefore, the assumption of the finite mass density of the ions at the inlet is consistent. Before we subject the equations to numerical simulation, we have normalized the spatial scale with respect to the channel length L = 3.0 cm and temporal scale with respect to the ion-acoustic time, which for electron volt temperature, corresponds to 10^8 cm/s. The physical quantities are normalized with respect to some background quantities e.g., $\rho^* = \rho/\rho_0$ where ρ_0 is extracted from the observations.

Fig. 4 describes the ion streamlines. As is clear from the picture, after injection of the ion in the channel, it diverges toward the exit plane under the influence of electric and magnetic fields. In the absence of magnetic field, there will be no divergence and ions will be axially flushed out of the thruster. However, magnetic field plays here a dual role. On the one hand it confines the electron to the radial direction, inhabiting their axial motion, and on the other, it affects the ions motion. Since the plasma has a tendency to remain quasi-neutral, the moment ions moves axially, it feels an attractive space charge field locally which deviates its trajectory from a straight line. Therefore, even though, ions are not directly coupled to the magnetic feel, they interact with the field through the electrons - a situation not very different from ambipolar diffusion. Other than the effect of the magnetic field, the ion trajectory does not get significantly modified inside the channel. This is consistent with the fact that ions are cold. The charge exchange collisional ionization does not seem to affect the ions speed in any significant way. We anticipate that the non-uniformity in the ions speed will appear once the thermal pressure gradient is included in the ion dynamics. The result of this uniformity of ions speed will be that the ion density will remain uniform in space.

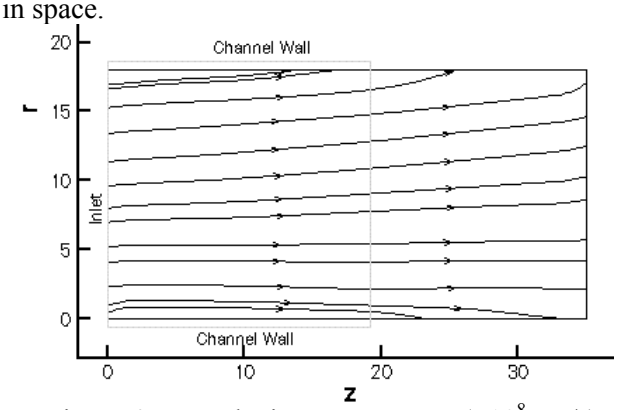

Figure 4. Ion velocity streamtraces (~10^8 cm/s).

The electron density profile is documented in Fig. 5. If we take the typical electron number density observed in the experiments [20] n_e~10^{11} cm^{-3}, then the corresponding simulation box density solution represents very low electron number density (~10^9), except near the inlet.

The axial and radial velocity profiles for the electron are shown in Fig. 6. From Fig. 6a we see that there is a considerable change in the magnitude of the axial velocity profile of the electron. This is reflective of the influence exerted by the dominant radial magnetic field, which inhibits the axial electron flow. The magnitude of the radial flow (Fig. 6b) on the other hand, does not change significantly. This is anticipated on the ground that the effect of magnetic force on the radial electron flow is much weaker due to the

smallness of the axial magnetic field. Multiplying the normalized velocity with the thermal velocity of the electron, we see that the bulk flow of electron fluid by an order of magnitude smaller near the inlet.

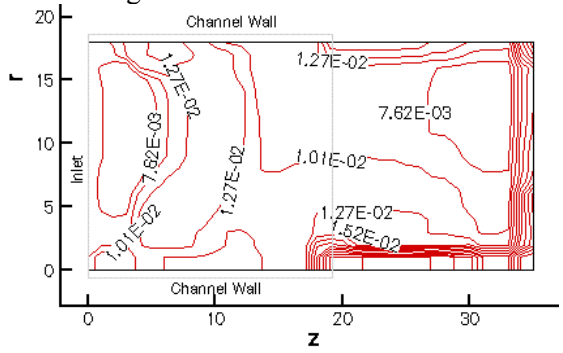

Figure 5. Electron density.

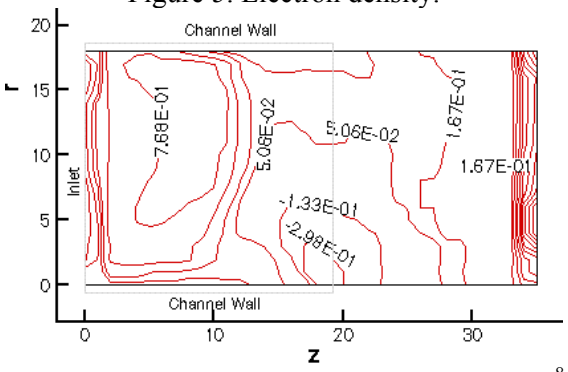

Figure 6a. Streamwise (z) electron velocity $\times 10^8$.

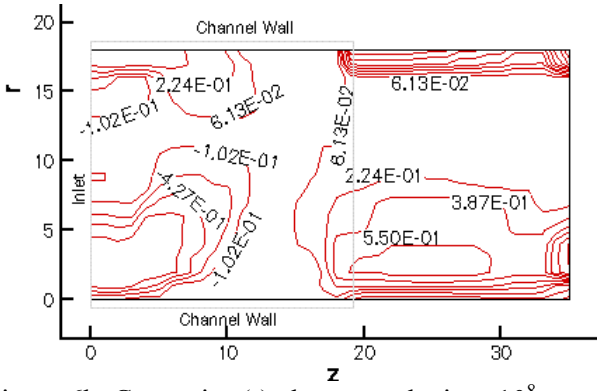

Figure 6b. Crosswise (r) electron velocity $\times 10^8$.

The electron velocity streamlines are given in Fig. 7. The effect of magnetic field is fully evident as electron streamlines are non-uniform. Pressure gradient and Lorentz force are operating simultaneously. The streamline density is high near the inlet suggesting that there is a sharp velocity gradient. As the role of boundary condition is crucial for the dynamics, we need to investigate the flow features observed here in the presence of wall sputtering as that will affect the velocity accumulation. This can be seen from the fact that sputtering and recombination will work as a source and sink of the energetic electrons.

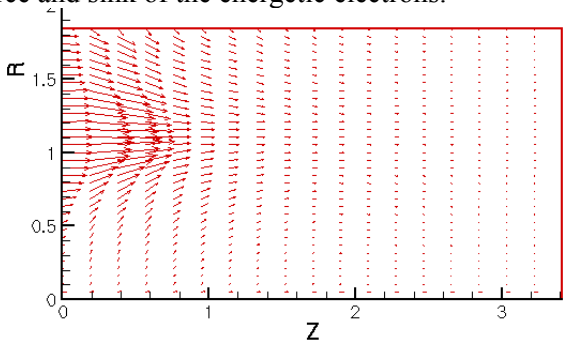

Figure 7. Electron Velocity.

We note that the spatial evolution of density (Fig. 5) is correlated with the temperature evolution (Fig. 8). In fact this correlation could be anticipated on the physical ground. The number of high energetic electrons will be less than the number of low energy electrons in any given distribution. Therefore, the region of high temperature should reflect a dip in the electron density. The typical electron temperature is in the range of few eVs, which compares favorably with the experimental observations [20]. The temperature peaks in the region where the radial magnetic field is the maximum. We

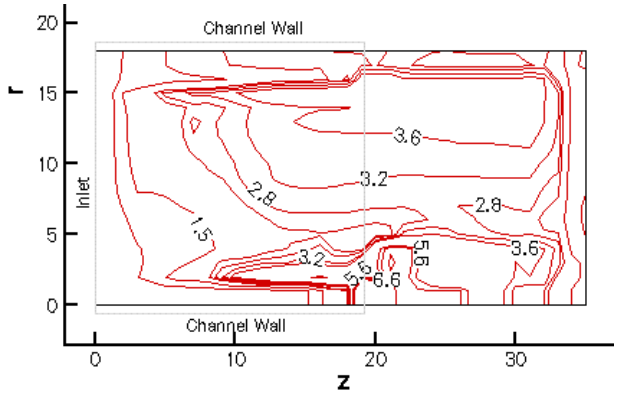

Figure 8. Electron energy (eV)

note however that the temperature contours are dissimilar to the one reported by Fife [6,12]. We attribute this dissimilarity to our difference in boundary condition assumptions. Further more in PIC model [6,12,15] a steady state plasma is considered while our TMST model is unsteady. Finally the thrust at the exit plane of NASA 120M is calculated and plotted as a function of time in Figure 9. The simulation result shows a final thrust of 101.4 mN that matched within 1% of the measured value [17].

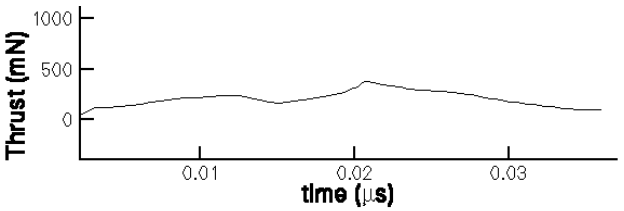

Figure 9. Calculated thrust for NASA 120M.

Conclusions

Present work describes the time-dependent plasma dynamics of a Hall thruster in the framework of a two fluid model. The model assumes that ions are cold and unmagnetized whereas electrons are energetic. The ions feel the effect of the magnetic field only through electrons and they are driven from anode to cathode by an externally imposed electric field. Within this simplified framework, we observe that the electron density and temperature inside the box is similar in magnitude to the experimental data [20]. Despite showing similar temperature range, the contour patterns and their locations are not in agreement with PIC results. This we attribute to the unsteady plasma model and our selection of boundary conditions.

The model calls for further generalization. First, the ion and electron temperature equations need to be solved simultaneously. Also, the effect of ionization and recombination needs to be incorporated in the model. We have noticed that the solutions are very sensitive to the initial as well as boundary conditions. Therefore, sputtering at the boundary is a major issue in the dynamics and requires to be addressed in our future work.

Acknowledgement

This work is supported by NASA GRC research Grant no. NAG3-2520 with Maris Mantenieks as the technical monitor. The authors gratefully acknowledge the support of Robert Jankovsky, Dave Manzella and Peter Peterson.

Reference:

1. V.V. Zurin, H.R. Kaufman and R.S. Robinson, Plasma Sources Sci. Technology, Vol. 8, p.R1-R20 (1999).
2. R. Jankovsky, S. Tverdokhlebov and D. Manzella, in 35th Joint Propulsion Conf., AIAA-99-2949 (1999).
3. V. Kim, J. Propulsion and Power, Vol. 14, p.736 (1998).
4. M. Keidar and Iain D. Boyd, Effect of a magnetic field on the plasma plume from Hall thrusters, J. of Applied Phys. V. 86, no 9, p.4786-4791, 1999.
5. I. D. Boyd, A review of Hall thruster plume modeling, AIAA paper 2000-0466, January 2000.
6. J. M. Fife, Hybrid pic modeling and electrostatic probe survey of Hall thrusters, Ph.D thesis, MIT, 1998.
7. K. Komurasaki and Y. Arakawa, Two-dimensional numerical model of plasma flow in a Hall Thruster, J. of Propulsion and Power, Vol. 11, pp. 1317-1323, 1995.
8. J. P. Boeuf and L. Garigues, Low frequency oscillation in a stationary plasma thrusters, J. of Applied Phys. Vol. 84, pp. 3541-3554, 1998.
9. E. Ahedo, P. Martinez and M. Martinez-Sanchez, Steady and linearly-unsteady analysis of a Hall Thruster with and internal sonic point, AIAA 2000-3655, January 2000.
10. I. D. Boyd, Computation of the plume of an anode layer Hall Thruster, J. of Propulsion and Power, Vol. 16, pp. 902-909, 2000.
11. C.K. Birdsall and A.B. Langdon, Plasma Physics Via Computer Simulation, Adam Hilger Press (1991).
12. J.M. Fife, M.S. Thesis, MIT (1995).
13. K.J. Berry and S. Roy, in 39th Aerospace Sciences Meeting, AIAA-2001-0200 (2001).
14. J.P. Boeuf and L. Garrigues, Journal of Applied Physics, Vol. 84, no. 7, p.3541, (1998).
15. I. Katz, M. Mandell and Y. Mikellides, 1-D HET code, (Internal memo to D. Manzella), Maxwell Tech. (2000).
16. S. Roy, Combining Galerkin matrix perturbation with Taylor weak statement algorithms, Computer Methods in Applied Mechanics and Engineering, Vol. 184, pp. 87-98, 2000.
17. D. Manzella and P. Peterson, Private communications, 2001.
18. D. Y. Oh, D. E. Hastings, C. M. Marrese, J. M. Hass and A. D. Gallimore, J. of Propulsion and Power, Vol. 15, pp. 345, 1999.
19. Y. Raitses, Ph.D thesis, Technion, 1997.
20. A.M. Bishaev and V. Kim, Local plasma properties in a Hall current accelerator with an extended acceleration zone, Soviet Physics, Technical Physics, Vol. 23, no. 9, pp. 1055-1057, 1978.